Analysis of the stress and deformation states in the vertical flat-jack test

Corrado Chisari[1], Lorenzo Macorini[2], Bassam Izzuddin[3], Claudio Amadio[4]

Biographical statements

Corrado Chisari is a Marie Curie Research Fellow at the Department of Civil and Environmental Engineering at Imperial College London. Since he received his PhD in 2015, he has worked as a researcher at the University of Trieste, Salerno and at Imperial College. His main research focus regards structural optimisation, structural identification, numerical modelling and testing of masonry and steel structures, design of advanced seismic devices. Since September 2017, he has been working at Imperial College London on the EU project "MultiCAMS - Multi-level Model Calibration for the Assessment of Historical Masonry Structures".

Lorenzo Macorini is a Reader in Structural Engineering at Imperial College London. After gaining his PhD in Structural Engineering at the University of Trieste (Italy), he was involved in scientific projects funded by both public organizations and private industries focusing on numerical and experimental investigations of existing and new structures. From 2008 to 2010, he held a Marie Curie Intra-European Research Fellowship at Imperial College. Currently he is part of the Computational Structural Mechanics Group working on numerical modelling and analysis of structures including masonry buildings and bridges under extreme loading conditions.

[1] Marie Skłodowska-Curie Individual Fellow, Department of Civil and Environmental Engineering, Imperial College London (UK), c.chisari12@imperial.ac.uk

[2] Reader, Department of Civil and Environmental Engineering, Imperial College London (UK), l.macorini@imperial.ac.uk

[3] Professor, Department of Civil and Environmental Engineering, Imperial College London (UK), b.izzuddin@imperial.ac.uk

[4] Full professor, Department of Engineering and Architecture, University of Trieste (Italy), amadio@units.it

Bassam Izzuddin is Professor of Computational Structural Mechanics and heads the CSM group at Imperial College London. Since joining Imperial in 1990, he has developed advanced nonlinear analysis methods for structures subject to extreme loading, and he has engaged in national/international collaborations with industry and fellow academics on applied structural engineering research utilising his program ADAPTIC. Besides major developments in detailed modelling, he has also developed a range of simplified analysis methods, which are currently being applied in design practice for offshore and building structures. His publication record exceeds 250 papers in leading international journals and conferences.

Claudio Amadio is Full Professor of Structural Engineering at the Department of Engineering and Architecture of the University of Trieste. He has more than thirty-year experience in teaching undergraduate and graduate courses, and was President of BSc and MSc in Civil Engineering, University of Trieste, as well as Director of the Master in Earthquake Engineering, Gorizia, Italy. His research expertise, including glass, steel and composite structures, timber, earthquake engineering, finite element method, numerical modelling, bomb blast and experimental research, is summarised in more than 220 papers. Prof. Amadio is also a registered professional engineer

Abstract

Performing a realistic assessment of unreinforced masonry structures involves designing and executing appropriate experimental tests on masonry components for determining the material model parameters to be used in structural analysis. Considering recent developments in which inverse analysis was used as calibration framework, a vertical flat-jack test is investigated in this paper. Two simplified models are described for the analysis of the stress state in the masonry due to the pressure transferred by the flat-jack. Furthermore, with the aim of designing the sensor setup for the test, a POD analysis on the deformation state of the structure is carried out, highlighting the basic deformation modes which govern the response. The results show that high stresses and local modes can occur in the proximity of the flat-jack, and thus local use of FRP reinforcement is recommended to avoid undesired brittle crack propagation which may prevent accurate calibration of mortar joint mechanical characteristics.

Keywords: stress; deformation; vertical flat-jack; unreinforced masonry; structural assessment; Proper Orthogonal Decomposition; FRP reinforcement; sensor placement; mesoscale modelling; calibration; elastic properties; cohesion; friction coefficient; fracture energy.

1 Introduction

Unreinforced masonry (URM) structures, which constitute a large part of the existing built heritage, are characterised by a complex behaviour under extreme loading, mainly because of URM inherent heterogeneous nature and nonlinear behaviour. In the recent past, significant research has been devoted to the development of accurate numerical models for the structural assessment of URM structures, from micro-models (Lotfi & Shing, 1994; Lourenço & Rots, 1997; Gambarotta & Lagomarsino, 1997), where individual components, i.e., units and mortar, are explicitly modelled, to macroscale descriptions (Lourenço, et al., 1997; Papa, 1996; Berto, et al., 2002; Pelà, et al., 2011), in which a fictitious homogeneous material is considered and the material characteristics are obtained by the homogenisation of suitable micro-scale representations (Anthoine, 1995; Cecchi, et al., 2005; Milani, et al., 2006; Luciano & Sacco, 1997). Although detailed numerical models can in principle satisfactorily describe the behaviour of masonry taking into account its basic mechanical characteristics (anisotropy, softening, dilatancy, crack opening-closure and propagation, etc), they rely on a number of material parameters, the definition of which should precede any numerical analysis determining its success. However, no material parameter can be recorded directly, as parameter calibration generally implies the analysis of the results of specific experimental tests, where a set of response characteristics are recorded. Consequently, material tests can be defined as inverse problems, where a response is measured and then, based on an inverse model, the parameters determining that response are estimated.

Binda et al. (Binda, et al., 2000) report an extensive survey of different types of in-situ investigation procedures for masonry structures. In general, structural assessment undergoes different stages, from measuring the geometrical characteristics of the structure and surveying the crack pattern by means of visual inspections to the estimation of the stress state and calibration of material parameters. In-situ tests on large portions of walls provide extensive information about strength and deformability of masonry (Corradi, et al., 2003; Borri, et al., 2011). However, because of their invasiveness (during the

test walls are often extensively damaged), technical challenge and cost, these methods are currently performed only in a few cases, and less destructive and expensive strategies are usually preferred. In (Mazzotti, et al., 2014) and (Sassoni, et al., 2014) some low-invasive techniques for retrieving shear and compressive masonry strength are described. An extensive comparison between several testing methods for shear failure parameters is reported in (Ferretti, et al., 2019).

The "inverse model" mentioned above, being the bridge between what is observed and what is to be calibrated, plays a crucial role in the calibration process. From a conceptual point of view, if the assumptions of a specific numerical description allow for a "satisfactory" representation of a certain behaviour of a physical process, there is no reason to estimate the parameters entering its formulation by using different assumptions. On the contrary, it seems natural to apply techniques from the field of the Inverse Problem theory (Tarantola, 2005) to calibrate those parameters. In the literature, many works regard the characterization of Young modulus of masonry assumed as a homogeneous material, by means of dynamic tests (D'Ambrisi, et al., 2012; Gentile & Saisi, 2007). (Calderini, et al., 2010) propose an inverse analytical procedure based on Mann and Muller's model to identify cohesion and friction angle from the results of a diagonal compression test. Micro- and meso-models require a larger number of input material parameters to be identified in order to characterize the behaviour of the masonry. It is common practice to determine such material parameters from the results of various, relatively simple, small scale laboratory experiments (Andreotti, et al., 2018; Marastoni, et al., 2016). However, masonry is a highly variable, stress-state dependent material which experiences non-uniform distributions of stress in real structures. Moreover, boundary conditions in small scale tests are unlikely to be representative of those found in a larger structure. These considerations have cast doubts on the effectiveness of determining material parameters representative of masonry from small scale experiments, and thus in (Morbiducci, 2003; Sarhosis & Sheng, 2014; Chisari, et al., 2018) inverse analysis procedures are applied to large scale tests to obtain material parameters for different detailed masonry models.

A vertical flat-jack test for the calibration of mesoscale material parameters is proposed in (Chisari, et al., 2015) and in (Chisari, et al., 2018), where a comprehensive framework including experimental testing, sensitivity and inverse analysis is presented and discussed. This model calibration strategy showed significant potential. However, given the complexity of the topic, some important details regarding design choices as the absence of lateral restraints, application of FRP reinforcement and sensor selection were omitted. In particular, as the aim of the test is to calibrate material properties of mortar joints, special attention needs to be paid to the development of appropriate crack patterns involving damage in mortar rather than in bricks. These aspects are covered in the present work, where a further analysis on the stress and deformation states, which develop in the flat-jack test, is described. After a general description of the framework, the mesoscale material model for masonry and the experimental setup, two simplified linear models are proposed to analyse the stress state induced by the flat-jack. A POD analysis on the deformation field is then presented with the aim of capturing the most important features of the response that should be measured by the sensors. Based on the outcomes of this analysis, a suitable sensor setup is then proposed.

2 Summary of the calibration procedure

2.1 Overview

The calibration procedure proposed in previous research (Chisari, et al., 2015; Chisari, et al., 2018) is based on the use of inverse analysis for the post-processing of data $\boldsymbol{d_{obs}}$ obtained in an experimental test to determine the parameters $\boldsymbol{m}$ of a model $g(\boldsymbol{m})$ (forward operator) assumed capable of describing the observed structural response. The forward operator is generally represented by a numerical (Finite Element) or analytical model. The measurable entities used for the masonry application herein considered are displacements. Supposing that an inverse operator g^{-1} exists, the deterministic inverse problem reads:

$$\tilde{\boldsymbol{m}} = g^{-1}(\boldsymbol{d_{obs}}) \quad (1)$$

The explicit form of the inverse operator is usually unknown, and it is common to solve (1) by turning it into a minimisation problem:

$$\tilde{\boldsymbol{m}} = arg\min_{\boldsymbol{m}} \omega\left(\boldsymbol{d_{obs}}, g(\boldsymbol{m})\right) \quad (2)$$

where $\omega\left(\boldsymbol{d_{obs}}, g(\boldsymbol{m})\right)$ is a suitable discrepancy function measuring the inconsistency between the measured data $\boldsymbol{d_{obs}}$ and the computed counterparts $g(\boldsymbol{m})$.

While some properties of the forward operator as existence, uniqueness and stability hold in most cases, they are not usually satisfied for inverse problems. Different regularisation strategies (Tikhonov & Arsenin, 1977; Kabanikhin, 2008) are thus needed, including more recent approaches which investigate robustness along with fidelity (Atamturktur, et al., 2014) or consider alternative definitions of the inverse problem solutions (Fernández-Martínez, et al., 2013; Chisari, 2018).

This paper investigates some specific aspects of the experimental test proposed by the authors for the calibration of a specific mesoscale model for brick/block masonry. Both the numerical model and the test are briefly presented in the next subsections. Conversely, some other details of the adopted inverse analysis framework, including the selection of the parameters to calibrate by means of sensitivity analysis and the use of surrogate models to decrease the computational effort, are not discussed and the reader is referred to (Chisari, et al., 2018) for further information.

2.2 The mesoscale model

The forward problem which provides the output $g(\boldsymbol{m})$ given the parameters $\boldsymbol{m}$ is a FE model representing the experimental test. In the mesoscale approach employed in this work (Macorini & Izzuddin, 2011), a masonry element is modelled by explicitly representing units and mortar joints. Mortar and unit–mortar interfaces are lumped into 2D 16-noded zero-thickness interface elements. Masonry units are described by elastic 20-noded solid elements, and possible unit failure in tension and shear is accounted for by means of the nonlinear behaviour of zero-thickness interface elements

placed at the vertical mid-plane of each block (Figure 1). The discretisation for the structure, as proposed in (Macorini & Izzuddin, 2011), consists of two solid elements per unit connected by a unit-unit interface.

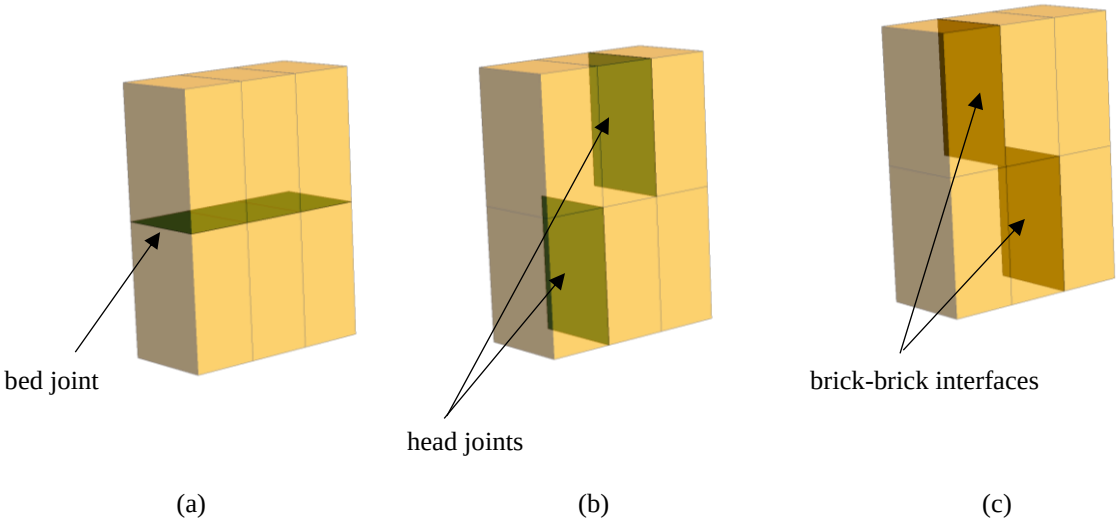


Figure 1. Mesoscale modelling of masonry by means of elastic solid elements for units (in transparency) and zero thickness interfaces: (a) bed joints, (b) head joints, and (c) brick-brick interfaces.

The interface local material model is formulated in terms of one normal and two tangential tractions $\boldsymbol{\sigma} = \{\tau_x, \tau_y, \sigma\}^T$ and relative displacements $\boldsymbol{u} = \{u_x, u_y, u_z\}^T$ evaluated at each integration point over the reference mid-plane. In the linear range, they are linked to one another by uncoupled elastic stiffnesses, which simulate the linear elastic response of mortar joints, $\boldsymbol{\sigma} = \boldsymbol{k}\,\boldsymbol{u}$. As mentioned before, interface elements with nonlinear constitutive model are employed also to represent potential cracks within masonry units, and in this case a large elastic stiffness is used as a penalty factor to prevent penetration and separation before cracking between elastic solid elements representing different portions of individual masonry brick/blocks. The description for the nonlinear behaviour is based on a plastic work-softening formulation, characterized by one hyperbolic yield function F_1 to simulate Mode I and Mode II fracture, which provides a smooth transition between pure tension and shear failure:

$$F_1 = \tau_x^2 + \tau_y^2 - (c - \sigma\, tan\phi)^2 + (c - \sigma_t\, tan\phi)^2 = 0 \qquad (3)$$

The three parameters c, σ_t, $tan\phi$ associated with surface F_1 represent cohesion, tensile strength and friction coefficient at mortar interface. The interface material model for mortar joints employs a second hyperbolic function F_2, the cap in compression, to account for masonry crushing:

$$F_2 = \tau_x^2 + \tau_y^2 - (\mathrm{D} - \sigma\ tan\theta)^2 + (D - \sigma_c\ tan\theta)^2 = 0 \qquad (4)$$

where σ_c is the compressive strength and D, θ are additional material parameters. Both surfaces F_1 and F_2 shrink with the development of plastic work, following an evolution law governed by the fracture energy, which is assumed as characteristic property of the material. Three fracture energies are to be defined to fully characterise the nonlinear response of the interface: $G_{f,I}$ for mode I (tension) failure, $G_{f,II}$ for mode II (shear) failure, and $G_{f,C}$ for failure in compression. It is assumed that when the dissipated energy equals the fracture energy, cohesion, tensile strength and friction coefficient reach some residual values, which represent additional material characteristics. The material model is implemented in the FE software ADAPTIC (Izzuddin, 1991).

2.3 The vertical flat-jack test

Flat-jacks are commonly used for testing existing masonry under compression (Binda & Tiraboschi, 1999; Gregorczyk & Lourenço, 2000). An interesting application for retrieving shear strength properties of the masonry as a continuum is proposed in (Caliò, 2011). According to this approach, the flat-jack is arranged vertically and a cut parallel to it enables the translation of the masonry portion subjected to the horizontal pressure exerted by the flat-jack. Another innovative use of flat-jacks is described in (Garbowski, et al., 2011). In this study, flat-jacks are arranged both in the horizontal and vertical direction and inverse procedures are employed to calibrate elastic parameters of concrete dams, leading to realistic estimates of the horizontal and vertical deformability of concrete assumed as orthotropic material.

Considering these previous contributions, an experimental setup was developed in (Chisari, et al., 2015; Chisari, et al., 2018). It consists of a non-conventional shear test on a masonry wall, where two

flat-jacks are used to apply a controlled pressure along the vertical and horizontal direction (Figure 2a). In a preliminary setup, described in (Chisari, et al., 2015), after the horizontal cutting along a portion of a mortar bed joint of the wall (phase 1), a horizontal flat-jack is placed to apply a known compressive stress (phase 2), like in a standard single flat-jack test, but not necessarily up to balance the stress originated by self-weight of the part of the structure above the cut. Afterwards, the pressure in the horizontal flat-jack is maintained constant, while the lateral faces of the masonry panel are restrained to prevent any horizontal displacements (Figure 2a). Two vertical cuts of equal length are then executed in the area underneath the horizontal flat-jack and a vertical flat-jack is placed in either vertical cut (right cut in Figure 2a). Thus, an approximately square panel can be tested under shear by increasing the pressure in the vertical flat-jack (phase 3) which gives rise to a displacement field within the panel where the empty cut (vertical cut in Figure 2a) is closing.

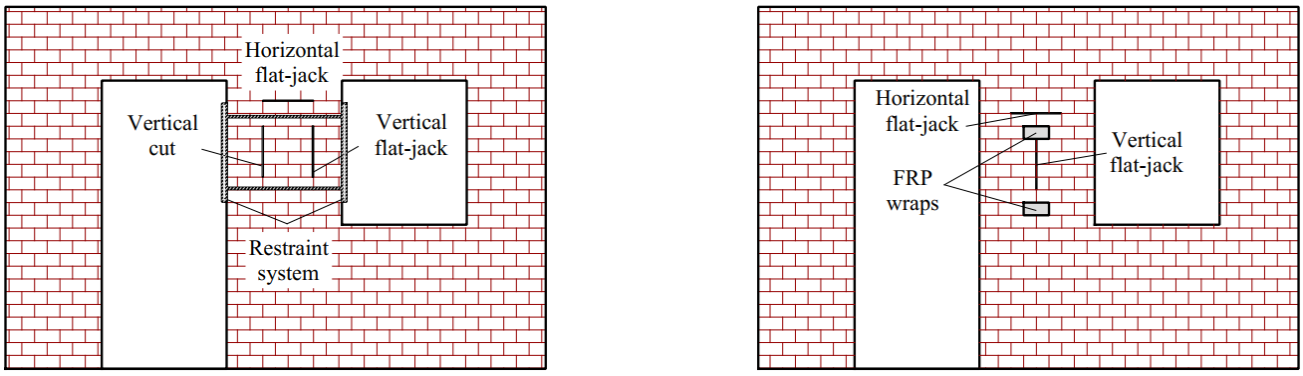


Figure 2. Schematic diagram of (a) the preliminary and (b) the simplified setups.

This setup was then simplified in (Chisari, et al., 2018) by removing the constraint system and the vertical cut (Figure 2b). Additional FRP wraps were designed to limit the spread of undesired vertical cracks, as described in the next Section.

In the next Sections an in-depth analysis of the stress state will highlight the main feature of the test and justify the choices of both simplifying the setup and adding the local reinforcement as proposed in (Chisari, et al., 2018). The analysis of the deformation field will also uncover the main deformation

modes which need to be captured by the sensors on the specimen in order to fully describe the overall response.

3 Analysis of the stress state

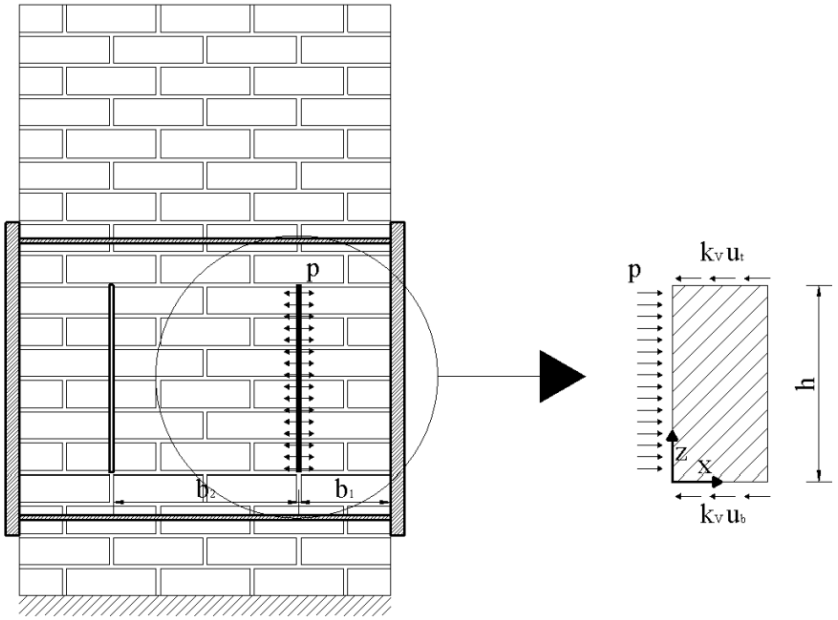
3.1 Tangential stresses in the mortar joints

The application of a flat-jack in a vertical cut of the masonry structure may be studied by means of an approximate analytical model in the elastic range. Consider the portion of the *t* thick panel identified by the *h* high vertical cut and the two horizontal mortar layers of shear stiffness k_V (Figure 3), it is possible to write the horizontal translation equilibrium equation for the elementary segment of length *dx* identified by the coordinate *x* as:

$$N(x) + dN - k_V t[u_b(x) + u_t(x)]dx - N(x) = 0 \tag{5}$$

where $N(x) = \int_o^t \int_o^h \sigma_x dydz$, and $u_{b(t)}(x)$ is the horizontal relative displacement between the two faces of the bottom (b) or top (t) mortar layer. Considering the masonry element as a homogeneous isotropic continuum, the constitutive law can be expressed as:

$$\sigma_x = \frac{E}{(1-2v)(1+v)}\left[(1-v)\varepsilon_x + v\left(\varepsilon_y + \varepsilon_z\right)\right] \approx E\varepsilon_x = E\frac{\partial u_x}{\partial x} \tag{6}$$



215

216 Figure 3. Schematisation of the panel subjected to the vertical flat-jack pressure.

217 So, the panel axial force $N(x)$ is given by:

$$N = \int_o^t \int_o^h \sigma_x dy dz = \int_o^t \int_o^h E \frac{\partial u_x}{\partial x} dy dz \tag{7}$$

218 If we assume that u_x is linear in z, that is $u_x = u_b + \frac{u_t - u_b}{h} z$, eq. (7) becomes:

$$\begin{aligned} N &= E \frac{\partial}{\partial x} \int_o^t \int_o^h \left(u_b + \frac{u_t - u_b}{h} z \right) dy dz \\ &= Et \frac{\partial}{\partial x} \int_o^h \left(u_b + \frac{u_t - u_b}{h} z \right) dz = Eth \frac{\partial}{\partial x} \frac{u_t + u_b}{2} \\ &= Eth \frac{d}{dx} \frac{u_t + u_b}{2} \end{aligned} \tag{8}$$

219 since $\int_o^h \left(u_b + \frac{u_t - u_b}{h} z \right) dz = u_b h + \frac{1}{2h} [(u_t - u_b) z^2]_0^h = \frac{h}{2} (u_t + u_b)$ and the partial derivative may

220 be transformed into the total derivative. So, expressing N(x) in eq. (5) by eq. (8) leads to the differential

221 equation describing the problem:

$$Eth \frac{d^2}{dx^2} \frac{u_t + u_b}{2} - k_V t (u_b + u_t) = 0 \tag{9}$$

222 that is a second-degree differential equation with constant coefficients:

$$\frac{d^2u}{dx^2} - \alpha^2 u = 0 \tag{10}$$

223 where $u = \frac{u_t+u_b}{2}$, $\alpha^2 = \frac{2k_V}{Eh}$.

224 Instead, if a parabolic trend is assumed for $u_x(z)$, that is:

$$u_x(x,z) = \frac{2}{h^2}[u_t(x) - 2u_m(x) + u_b(x)]z^2 + \frac{1}{h}[4u_m(x) - 3u_b(x) - u_t(x)]z + u_b(x) \tag{11}$$

225 where $u_m(x) = u_x\left(x, \frac{h}{2}\right)$, it is easy to prove that the differential equation becomes:

$$\frac{1}{3}\frac{d^2}{dx^2}(u + 2u_m) - \alpha^2 u = 0 \tag{12}$$

226 and assuming the shape of the deformation being constant in *x*, i.e. $\frac{u_m(x)}{u(x)} = k$, eq. (12) reads:

$$\frac{d^2u}{dx^2} - \beta^2 u = 0 \tag{13}$$

227 where now $\beta^2 = \frac{3a^2}{1+2k}$.

228 The solution is in the form:

$$u(x) = c_1 \sinh \beta x + c_2 \cosh \beta x \tag{14}$$

229 and from equation (8) we obtain the axial force on the panel:

$$N(x) = \frac{Eth}{3}(1 + 2k)\frac{du}{dx} = \frac{Eth}{3}(1 + 2k)\beta(\, c_1 \cosh \beta x + c_2 \sinh \beta x) \tag{15}$$

230 The constants c_1 and c_2 can be determined by imposing two boundary conditions. The first condition

231 is that at x=0, the axial force is the resultant of the compressive pressure forces transferred by the flat-

232 jack -N_m:

$$N(0) = -N_m = \frac{Eth}{3}(1 + 2k)\beta c_1 \;\rightarrow\; c_1 = -\frac{3N_m}{Eth\beta(1 + 2k)} \tag{16}$$

233 For the second condition, we can consider two possibilities. The first is that, as on the right of the flat-

234 jack in the setup considered in Figure 3, at a distance b_1 we have a constraint on displacements:

$$u(b_1) = c_1 \sinh \beta b_1 + c_2 \cosh \beta b_1 = 0$$
$$c_2 = -c_1 \tanh \beta b_1 \tag{17}$$

The second possibility is, as on the left of the flat-jack in the setup considered in Figure 3, at a distance b_2 there is a free edge:

$$N(b_2) = \frac{Eth}{3}(1 + 2k)\beta(c_1 \cosh \beta b_2 + c_2 \sinh \beta b_2) = 0$$
$$c_2 = -c_1 \coth \beta b_2 \tag{18}$$

Whichever boundary condition is used, it is possible to evaluate $u(x)$ and $N(x)$. The single displacements u_b, u_t may be determined by imposing the rotation equilibrium equation; if the flat-jack is centred with respect to the vertical cut, it may be assumed $u_b = u_t = u$.

Lastly, a remark regarding the definition of the panel Young modulus E is needed. Since the panel is actually anisotropic, it should be identified with the horizontal elastic modulus E_x. In a simplified way, neglecting the contribution of the bed joint shear behaviour on the panel stiffness, the brick and vertical mortar joints act as springs in series, so the displacement $u_{m,x}$ between two points horizontally spaced L caused by a horizontal force F may be evaluated as:

$$u_{m,x} = \frac{FL}{A_{bx}E_b} + \frac{Fn_m}{k_{N,hj}A_{bx}} = \frac{FL}{E_x A_{b,x}} \tag{19}$$

where the vertical joint has been considered as zero-thickness interface with axial stiffness equal to $k_{N,hj}$, and A_{bx}, E_b, n_m are respectively the area of the brick face of normal x, the brick Young modulus and the number of mortar joints in L. Approximating $n_m \approx \frac{L}{l_b}$, with l_b being brick stretcher dimension, we obtain the equivalent Young modulus in x-direction:

$$E_x = \left(\frac{1}{E_b} + \frac{1}{k_{N,hj}l_b}\right)^{-1} \tag{20}$$

that can be conveniently used in eqs. (15)-(18).

3.1.1 Validation and discussion

A 1310×1960×120mm^3 wall was modelled by using the mesoscale representation, in which each 250×120×55mm^3 brick is split into two 20-node elastic solid elements. Brick Young modulus was set equal to E_b=11000MPa, while two sets of mortar properties were considered in the analysis:

- Soft mortar: $k_{N,bj}$=100N/mm^3, $k_{V,bj}$=40N/mm^3, $k_{N,hj}$=50N/mm^3, $k_{V,hj}$=20N/mm^3;
- Stiff mortar: $k_{N,bj}$=1000N/mm^3, $k_{V,bj}$=400N/mm^3, $k_{N,hj}$=500N/mm^3, $k_{V,hj}$=200N/mm^3;

where k_N, k_V are the axial and the shear mortar interface stiffnesses, and the subscripts *bj* and *hj* refer to bed joint and head joint properties, respectively. A 250mm wide vertical slot was created in order to apply a vertical flat-jack pressure p=1MPa. The right vertical edge was fully restrained, to simulate the presence of a constraint as depicted in Figure 3; the left edge was assumed free. In this way, both boundary conditions for the analytical model studied in the previous subsection are represented. The model and the mortar joint arrangement are displayed in Figure 4.

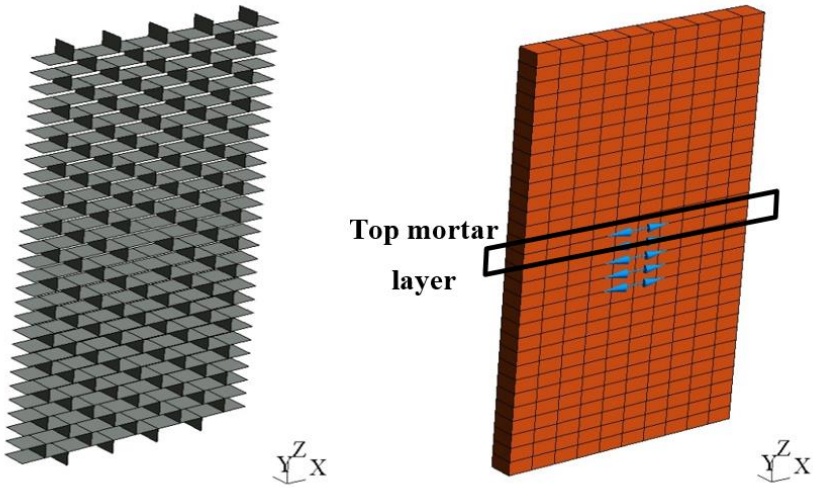


Figure 4. Numerical model for validation of the vertical flat-jack analytical description: (a) mortar arrangement and (b) complete model.

The comparison between numerical and analytical horizontal displacements of the mortar layer highlighted in Figure 4b is displayed in Figure 5. For the evaluation of the analytical response, the ratio k between u_m and u_t (the latter being assumed equal to u_b) must be estimated. In this case it has

been evaluated directly from the numerical response: its value is equal to 2.31 for the soft-mortar model and equal to 5.25 for the stiff-mortar model. With these values, the numerical response is generally well captured by the analytical model, except from the peak at the origin, which is underestimated.

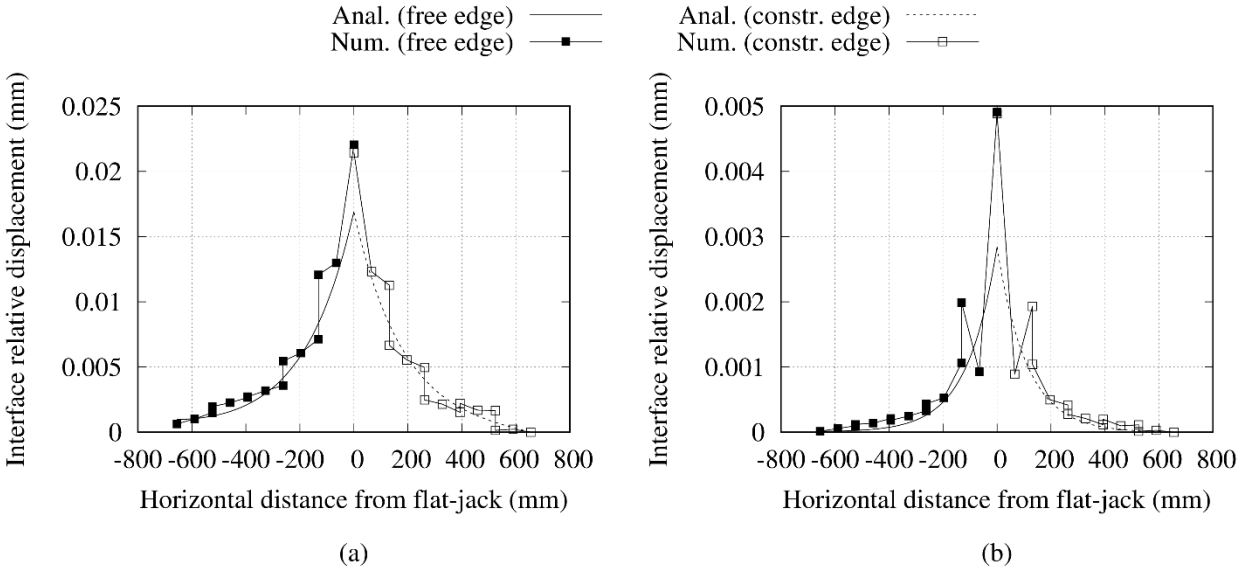


Figure 5. Comparison between numerical and analytical displacements on the mortar interface: (a) deformable mortar, (b) stiff mortar.

The simplified analytical model allows some remarks. The flat-jack action is auto-equilibrated, thus its effects vanish at a certain distance from the slot according to the Saint-Venant's principle. In this example, for the constrained edge and stiff mortar model, at the end of the wall, the reaction is equal to:

$$N(b_1) = \frac{Eth}{3}(1+2k)\beta(\, c_1 \cosh \beta b_1 + c_2 \sinh \beta b_1) = 156N \qquad (3.21)$$

about 0.5% of $N(0)$=1MPa×250mm×120mm=30kN. Thus, if the flat-jack is sufficiently far from the edge, there is no need for a constraint system as the one depicted in Figure 3, since the stress distribution is not affected by the constraint. In Figure 6a interface stress distributions, considering a free and a constrained edge as boundary conditions respectively, are compared. Here, the flat-jack is 655mm far from the vertical edge (assuming the material properties described for the soft-mortar

model): the stresses are almost coincident. In Figure 6b, maintaining the same masonry properties, the flat-jack is assumed to be 250 mm far from the border. Now the two distributions are different, even if the maximum stress is rather similar. When mortar is very deformable, a situation as displayed in Figure 7 will appear: if present, the constraint absorbs much of the stress and consequently the compressive stresses transferred by the flat-jack decay very slowly (Figure 7b).

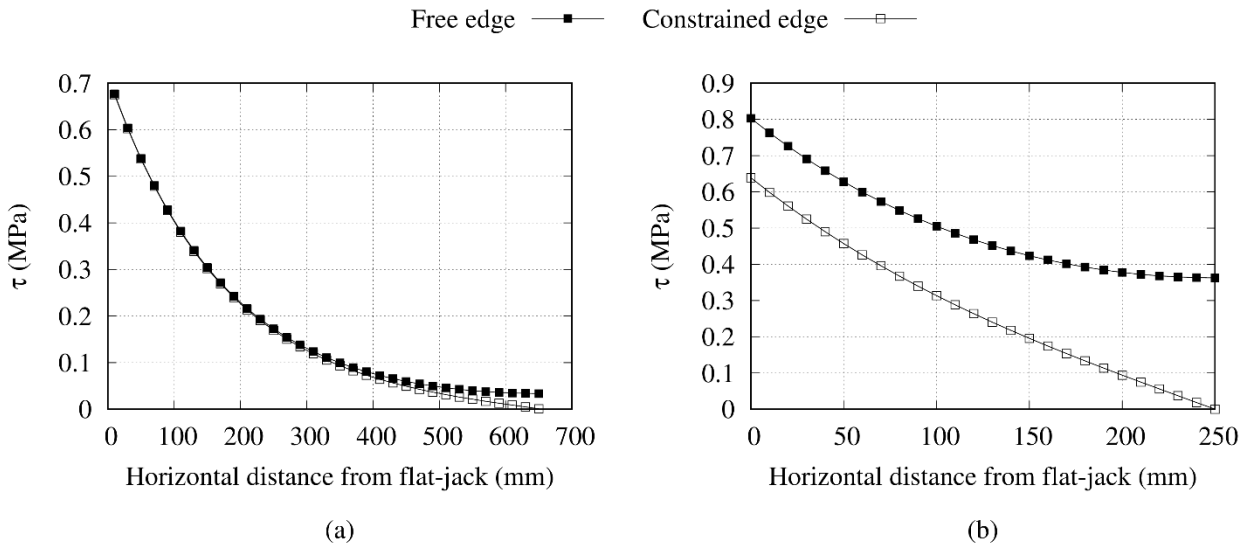


Figure 6. Tangential stress distribution for a flat-jack (a) 655mm and (b) 250 mm far from the edge.

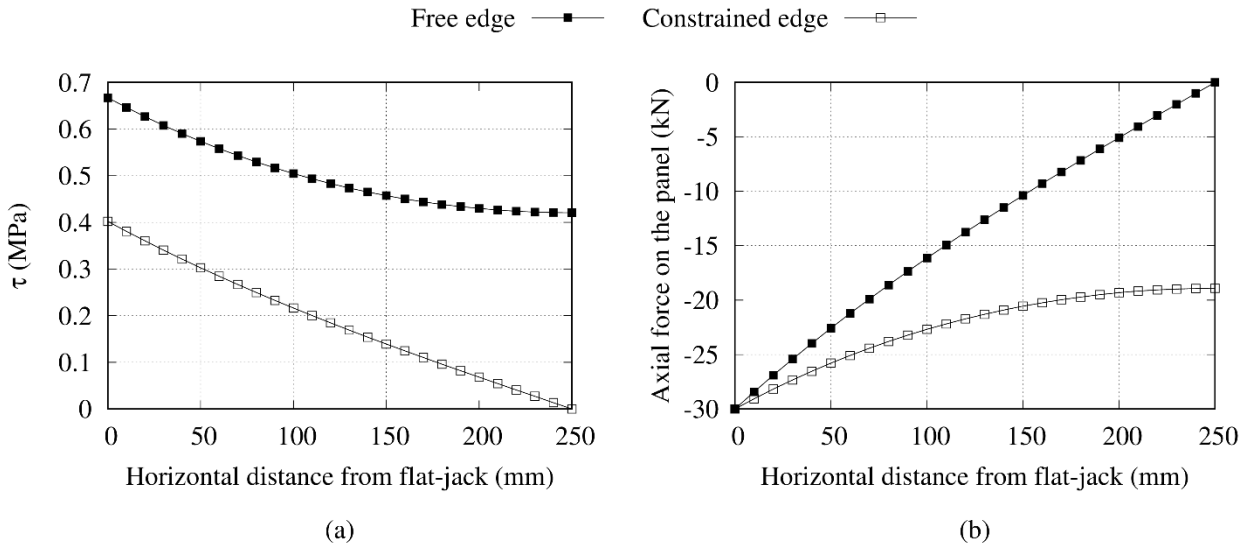


Figure 7. Very deformable mortar: (a) tangential stress distribution and (b) axial force in the panel.

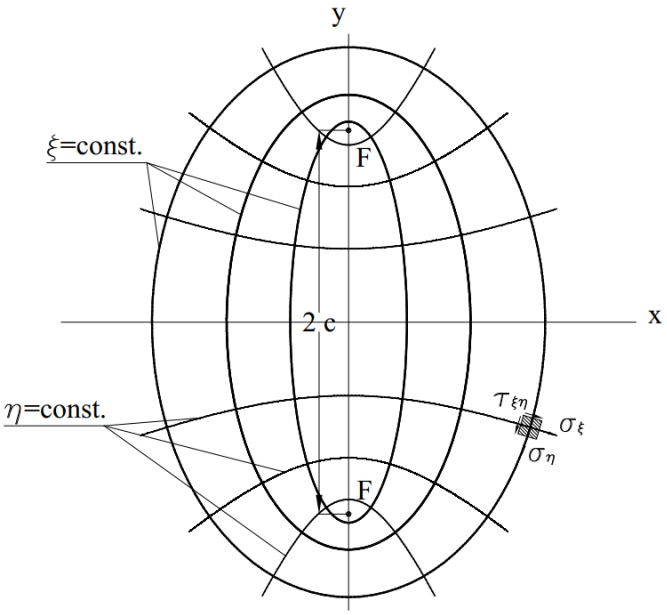
For the reasons described above, the constraint system and the empty vertical slot were removed in the simplified setup proposed in (Chisari, et al., 2018) (Figure 2b), and the vertical flat-jack applied symmetrically with respect to the horizontal flat-jack. This entails a considerable simplification in the overall setup, but it requires to control the tensile failure in the brick, as described in the following subsection.

3.2 Tensile stress in the bricks

An analytical solution for the general stress state can be developed if we consider an infinite plate made of a linear elastic homogenous material subjected to the flat-jack loading. The problem can be approached applying the superposition of the effects to the solution of a homogeneous infinite plate with an elliptic hole subjected to uniform horizontal uniaxial stress *p* (Coker & Filon, 1931; Oberti, 1947).

Let us consider an elliptic hole of focal distance *2c* and an elliptic reference system of coordinates (ξ, η) (Figure 8). The hole is identified by the parametric curve (ξ_0, η), and the Cartesian coordinates are related to the elliptic coordinates by the expressions:

$$\begin{aligned} x &= c \sin\eta \sinh\xi \\ y &= c \cos\eta \cosh\xi \end{aligned} \tag{22}$$



307

308 Figure 8. Elliptic hole and reference system.

309 The Airy function (in elliptic coordinates) solving the elastic problem is:

$$\chi = \frac{pc^2}{16}\{\chi_1 + (1 + 2e^{2\xi_0})\chi_2 + e^{4\xi_0}\chi_3 - 4(1 + \cosh 2\xi_0)\chi_4 + \chi_5\} \tag{23}$$

310 where χ_i i=1,…,5 are the following particular solutions of the biharmonic problem:

$$\begin{aligned} \chi_1 &= e^{2\xi} + \cos 2\eta \qquad \chi_2 = e^{-2\xi} + \cos 2\eta \\ \chi_3 &= e^{-2\xi}\cos 2\eta \quad \chi_4 = \xi \qquad \chi_5 = e^{2\xi}\cos 2\eta \end{aligned} \tag{24}$$

311 Substituting eqs. (24) in (23) and performing some transformations, we obtain:

$$\chi = \frac{pc^2}{8}\{\sinh 2\xi + [\cosh 2(\xi - \xi_0) - 1\ ]e^{2\xi_0}\cos 2\eta - 2\xi[1 + \cosh 2\xi_0] - e^{-2(\xi-\xi_0)}\} \tag{25}$$

312 It is of interest to study the situation when $\xi_0 = 0$, i.e. a cut with negligible thickness. In that case, the

313 Airy function becomes:

$$\chi = \frac{pc^2}{8}\{\sinh 2\xi + [\cosh 2\xi - 1\ ]\cos 2\eta - 4\xi - e^{-2\xi}\} \tag{26}$$

314 By differentiating the Airy function, the corresponding stresses in elliptic coordinates read:

$$\sigma_\eta = \frac{1}{h^2}\left\{\frac{\delta^2\chi}{\delta\xi^2} - \frac{1}{h}\frac{\delta h}{\delta\xi}\frac{\delta\chi}{\delta\xi} + \frac{1}{h}\frac{\delta h}{\delta\eta}\frac{\delta\chi}{\delta\eta}\right\}$$
$$\sigma_\xi = \frac{1}{h^2}\left\{\frac{\delta^2\chi}{\delta\eta^2} + \frac{1}{h}\frac{\delta h}{\delta\xi}\frac{\delta\chi}{\delta\xi} - \frac{1}{h}\frac{\delta h}{\delta\eta}\frac{\delta\chi}{\delta\eta}\right\} \quad (27)$$
$$\tau_{\xi\eta} = \frac{1}{h^2}\left\{\frac{\delta^2\chi}{\delta\xi\delta\eta} + \frac{1}{h}\frac{\delta h}{\delta\eta}\frac{\delta\chi}{\delta\xi} + \frac{1}{h}\frac{\delta h}{\delta\xi}\frac{\delta\chi}{\delta\eta}\right\}$$

where:

$$h^2 = \left(\frac{\delta x}{\delta\eta}\right)^2 + \left(\frac{\delta y}{\delta\eta}\right)^2 = \left(\frac{\delta x}{\delta\xi}\right)^2 + \left(\frac{\delta y}{\delta\xi}\right)^2 = c^2(\cosh 2\xi - \cos 2\eta) \quad (28)$$

We now want to investigate the stresses along the x and y axes, where for symmetry tangential stresses vanish. When *y*=0, $\eta = \frac{\pi}{2}$; hence:

$$\sigma_x = p\tanh^3\xi$$
$$\sigma_y = p\frac{\sinh 2\xi - 2}{2e^\xi\cosh^3\xi} \quad (29)$$

If *x*=0, instead, $\eta = 0$:

$$\sigma_x = p\coth\xi$$
$$\sigma_y = p\frac{\sinh^2\xi}{e^\xi\cosh^3\xi}; \quad (30)$$

The approximation of an infinite plate subjected to a uniform load -*p* with an elliptic hole represents the theoretical stress state on the structure subjected to a horizontal pressure when the cut is executed. Since the effect of the pressure applied by a flat-jack would be to restore the original unperturbed situation in which the stress state is characterised by $\sigma_x = -p$ and $\sigma_y = 0$ everywhere, we can write, assuming the superposition of effects holds:

$$\boldsymbol{\sigma}_{orig} = \boldsymbol{\sigma}_{cut} + \boldsymbol{\sigma}_{fj} \quad (31)$$

where $\boldsymbol{\sigma}_{orig}$, $\boldsymbol{\sigma}_{cut}$, $\boldsymbol{\sigma}_{fj}$ are the stress tensors of the original unperturbed state, due to the cut and the flat-jack, respectively. Hence, the stress state $\boldsymbol{\sigma}_{fj}$ due to a pressure applied by a flat-jack has normal components:

$$\sigma_x = p(\tanh^3 \xi - 1); \quad \sigma_y = p\frac{\sinh 2\xi - 2}{2e^{\xi}\cosh^3 \xi} \qquad \text{along x-axis}$$

$$\sigma_x = p(\coth \xi - 1); \quad \sigma_y = p\frac{\sinh^2 \xi}{e^{\xi}\cosh^3 \xi} \qquad \text{along y-axis} \tag{32}$$

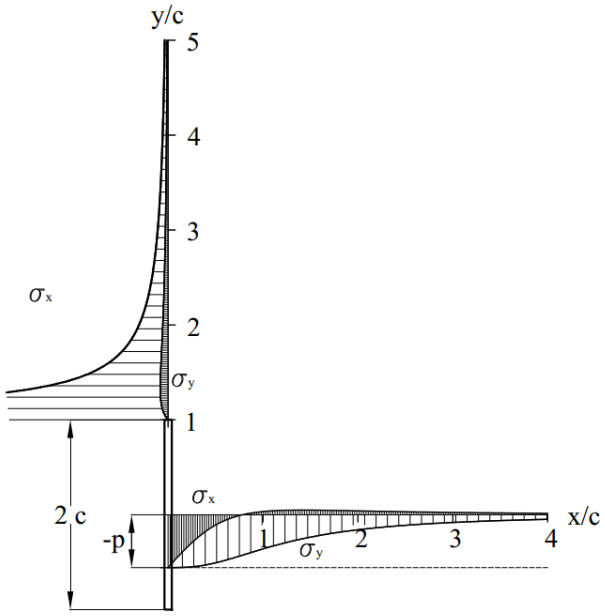
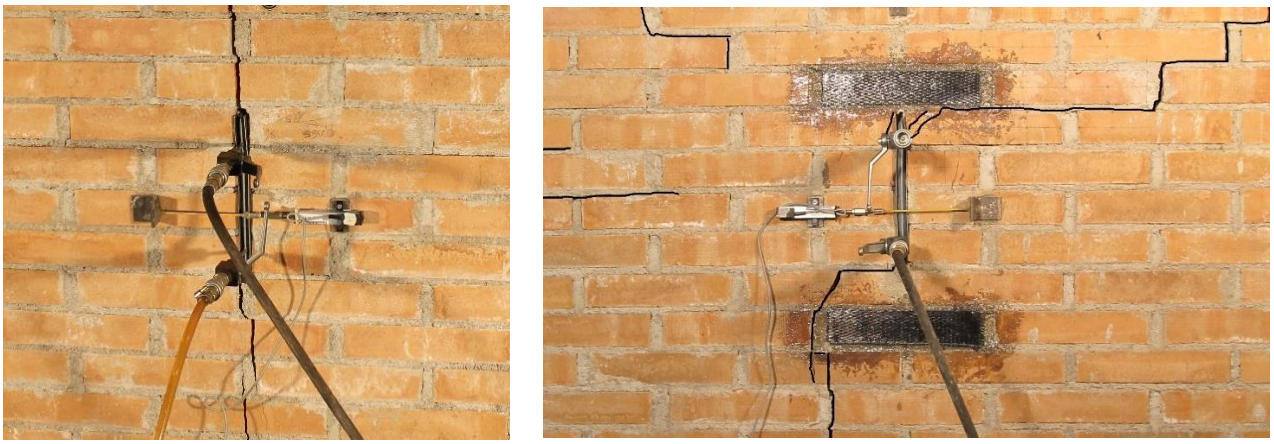


Figure 9. Stresses in the masonry due to the application of a constant stress by means of a vertical flat-jack.

This stress state is characterised by relatively small compressive stresses along the x axis with a maximum compressive stress of *-p* (Figure 9). On the contrary, very high tensile stress (theoretically infinite) can be reached along the y axis, in the proximity of the end point of the flat-jack.

The need of controlling such high stresses was apparent in a preliminary test, when vertical cracks developed along the direction of the flat-jack (Figure 10a). Such cracks are undesirable if the test results are used to identify the properties of mortar joints. In fact, strength and post-peak parameters of bed joints can be estimated using inverse analysis techniques only if they are effectively involved in the response, i.e. mixed tensile/shear failure in bed joints must be observed in the test. This clearly does not happen if cracks develop vertically, being hence governed by brick tensile strength. However, as high tensile stresses decay quite rapidly (they are less than *p* within a distance *c* from the flat jack, see Figure 9), the development of vertical cracks in the brickwork can be prevented by reinforcing the

bricks just above and below the slot. This can be achieved as suggested in (Chisari, et al., 2018) by means of CFRP strips glued to these bricks. In Figure 10 it is possible to notice that a completely different crack pattern can be generated in the specimen with reinforced bricks, which is characterised by failure of mortar joints in tension and shear and propagation of diagonal cracks. This enables the estimation of the nonlinear properties of the interfaces representing mortar joints by means of inverse analysis techniques.



(a) (b)

Figure 10. Crack pattern due to: (a) tensile failure of bricks during vertical flat-jack test; (b) shear and tensile failure of mortar joints.

4 Analysis of deformation field and sensor selection

The number and the position of sensors play a critical role in the solution of the inverse problem for the characterisation of the material properties of the masonry mesoscale model by means of the proposed vertical flat-jack test. This was already pointed out in (Chisari, et al., 2015), where the use of different arrangements of sensors was investigated by means of a pseudo-experimental approach. The results showed that errors up to 5% in a simple setup with 3 LVDTs per flat-jack (one horizontal and one vertical flat-jacks were considered to estimate elastic properties of interfaces modelling mortar joints) could lead to errors in the estimation up to 30%. It was also shown that using a full-field measurement system as DIC could greatly improve the solution.

The optimal sensor placement for the solution of the inverse problem can be obtained maximising the representativeness of the data with respect to the full field (Chisari, et al., 2016). Let us consider a vector field $\boldsymbol{u}(\boldsymbol{x})$, depending on the position $\boldsymbol{x}$; in the context of Finite Element Method, it can be written as a function of a vector of nodal values $\tilde{\boldsymbol{u}}$. The dependence of $\tilde{\boldsymbol{u}}$ on some material parameters $\boldsymbol{m}$ can be exploited by means of Proper Orthogonal Decomposition (POD) to define a reduced basis:

$$\tilde{\boldsymbol{u}}(\boldsymbol{m}) = \sum_{j=1}^{K} a_j(\boldsymbol{m})\, \boldsymbol{\varphi_j} = \boldsymbol{\Phi}\, \boldsymbol{a}(\boldsymbol{m}) \tag{33}$$

where $\boldsymbol{\Phi}$ is the $N \times K$ matrix representing the new basis of modes $\boldsymbol{\varphi_j}$, and $\boldsymbol{a}(\boldsymbol{m})$ is a vector collecting K amplitudes. If an experimental setup provides a limited set of nodal values $\boldsymbol{u_r}$, it can be shown that the global field can be expressed as:

$$\tilde{\boldsymbol{u}} = \boldsymbol{\Phi}\, \boldsymbol{\Phi_r}^{\dagger} \boldsymbol{u_r} = \boldsymbol{P} \boldsymbol{u_r} \tag{34}$$

where $\boldsymbol{\Phi_r}^{\dagger}$ is pseudo-inverse of matrix $\boldsymbol{\Phi_r}$ such that $\boldsymbol{u_r} = \boldsymbol{\Phi_r}\, \boldsymbol{a}$.

Equation (34) shows that a linear relationship between the experimental data and the global field can be established, and this can be used to select the position of the sensors to reduce the error propagation. In simpler terms, the sensors should be placed as to provide as much information as possible about the different deformation modes which characterise the response of the structure subjected to a specific test. These deformation modes are contained in matrix $\boldsymbol{\Phi}$ which can be evaluated by means of POD analysis.

4.1.1 POD analysis of the vertical flat-jack test

The test described in (Chisari, et al., 2018) has been considered here. The physical test was performed in laboratory on a 1310×1960×120mm^3 running bond masonry wall, made up of 250×120×55 mm^3 bricks, 10 mm thick horizontal mortar bed joints and 15 mm thick mortar head joints. The slot for the vertical flat-jack was prepared during the construction phase and filled with polystyrene sheets, to avoid cutting the panel. To be consistent with a potential in-situ application, a horizontal flat-jack was used to estimate vertical stresses induced by a hydraulic jack and distributed by a steel beam on the

top of the panel. Two 240×120×4 mm^3 rectangular flat-jacks were utilised. The vertical stress applied on the specimen and counterbalanced by the horizontal flat-jack was equal to 0.5MPa.

A nonlinear FE model of the specimen was developed considering a discretisation of the masonry texture following the approach described in Section 2. Thus, each brick was represented by two 20-noded solid elements connected by nonlinear 16-noded interface elements. Different interface material properties were used to model head and bed joints. Thanks to the geometrical and loading symmetry, only half specimen was discretised adding appropriate symmetry constraints. The elastic properties were determined from diagonal compression tests (Chisari, 2018) and were assumed fixed in the analysis. The Young's modulus of the brick was equal to E_b=13300MPa, while the head and bed joints were assumed rigid in the elastic range, as the apparent Young's modulus of mortar was similar to that of bricks. The nonlinear parameters ***m*** governing the model nonlinear response are those reported in Table 1, along with their variation ranges.

Table 1. Variation range for the strength material parameters.

Parameter	**Explanation**	**Lower bound**	**Upper bound**
f_{tb} (N/mm^2)	Brick tensile strength	0.5	7.0
$G_{fb,I}$ (N/mm^3)	Brick fracture energy (mode I)	0.01	0.25
c (N/mm^2)	Interface cohesion	0.1	1.8
$tan\phi$	Interface friction coefficient	0.45	1.5
σ_t (N/mm^2)	Interface tensile strength	$0.1 \cdot c$	$0.5 \cdot \frac{c}{tan\varphi}$
$G_{f,I}$ (N/mm^3)	Interface fracture energy (mode I)	0.005	0.02
$G_{f,II}$ (N/mm^3)	Interface fracture energy (mode II)	0.01 (with $G_{f,II} > G_{f,I}$)	0.25

By varying those parameters according to the Sobol quasi-random sequence (Sobol, 1967), 200 models were created and their response evaluated. It is well-known that the best exploration of the parameter space can be achieved by using a regular grid (full factorial design of experiments). However, the exponential increase in the number of samples at increasing number of dimensions makes the regular grid generally unfeasible for more than very few input parameters, especially when each evaluation implies the solution of a nonlinear Finite Element analysis as in the present case. The use of quasi-

399 random sequences allows for a good balance between computational effort and exploration of the
400 parameter space. Uncorrelated uniform distributions for each parameter were considered as no further
401 information was available on the material parameters. The number of models to analyse was dictated
402 by the need to limit computational time, and the same models then used for the creation of the surrogate
403 Kriging model were employed. It was shown in (Chisari, et al., 2018) that this allowed for a good
404 approximation of the global response.
405 The nodal displacement values for each time step of the analysis and each model were then collected
406 in the POD snapshot matrix $\bar{\boldsymbol{U}}$. The modal shape matrix $\boldsymbol{\Phi}$ can then be evaluated as (Chisari, et al.,
407 2016; Buljak, 2011):

$$\boldsymbol{\Phi} = \bar{\boldsymbol{U}}\boldsymbol{V}\boldsymbol{Z} \tag{35}$$

408 where:

409 • $\boldsymbol{V}$ is the $M \times K$ matrix whose columns are the first K eigenvectors of matrix $\boldsymbol{D}=\bar{\boldsymbol{U}}^{\boldsymbol{T}}\bar{\boldsymbol{U}}$;

410 • $\boldsymbol{Z}$ is the diagonal $K \times K$ square matrix whose elements z_{ii} are defined as:

$$z_{ii} = \lambda_i^{-1/2} \tag{36}$$

411 with λ_i being the i-th eigenvalue of matrix $\boldsymbol{D}$.
412 The overall deformation of the structure with varying material properties can be expressed as linear
413 combination of the modes contained in matrix $\boldsymbol{\Phi}$. These modes retain the most important features of
414 the structural deformation, as the POD basis is evaluated by minimising the average error in the
415 snapshot set.
416 It can be proved (Chisari, et al., 2016) that the error in the snapshot response, when generated using a
417 number $K<M$ of modes, is:

$$s = \sqrt{1 - \frac{\sum_{i=1}^{K} \lambda_i}{\sum_{i=1}^{M} \lambda_i}} \tag{37}$$

418 In the present case the error s lies below 1% with $K \geq 12$ (Figure 11).

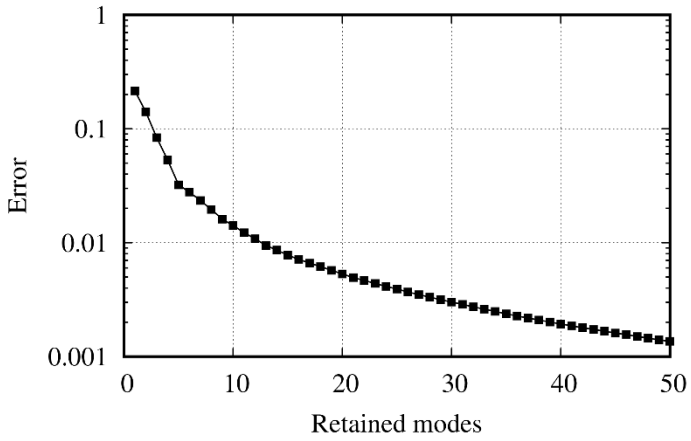


Figure 11. Truncation error due to POD approximation.

The first six modes are displayed in Figure 12. The first mode essentially represents the elastic deformation, which is equal in all the models of the snapshot set, as they all have the same elastic characteristics. Mode 2 is responsible for the formation of vertical cracks, which thus can be reduced but not completely avoided by the application of the FRP reinforcement. This can also be noticed in the bottom crack in Figure 10b. Modes 3-5 govern the formation of diagonal cracks and the horizontal crack on the left edge of the wall in correspondence of the midpoint of the flat-jack. Interestingly, both Mode 3 and 4 have a characteristic convex deformation near the application of the flat-jack which counterbalances the concave pattern seen in Mode 1. Most visible differences between them regard the pattern just below and above the flat jack (with the creation of vertical cracks in Mode 4). On the contrary, in Mode 5 the region in contact with the flat-jack is characterised by rigid rotation and translation, with negligible relative displacements between stacked bricks. Finally, Mode 6 is characterised by local deformations above and below the flat-jack.

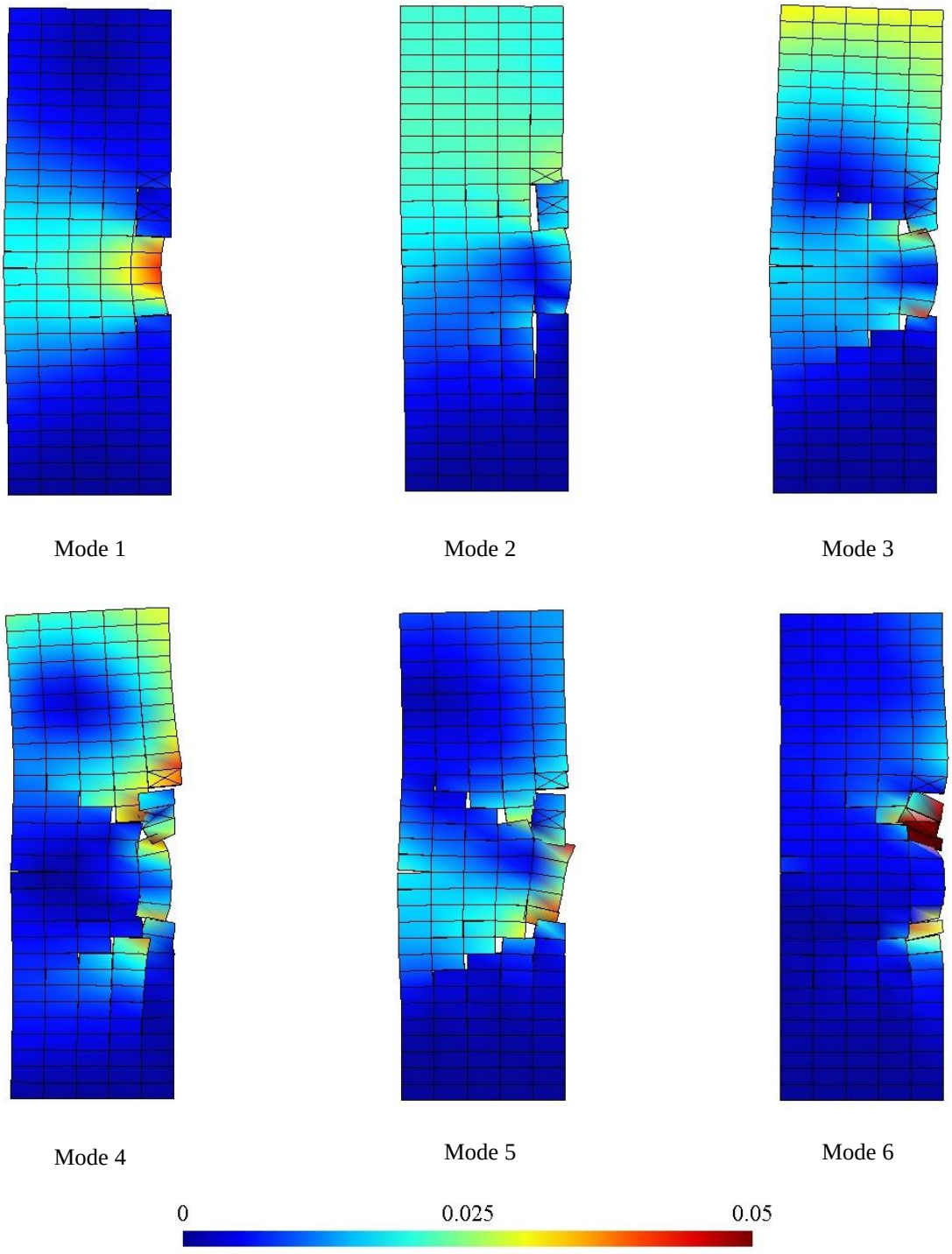


Figure 12. Deformation modes for the vertical flat-jack test (half wall is represented). The modes are orthonormalized and the scale factor for representation is equal to 1000.

This analysis confirms that the regions above and below the vertical cut are critical, as local deformations and cracks can be initiated due to high stresses. It also shows that vertical cracks can be initiated eccentrically with respect to the vertical flat-jack (Mode 2). Analogously to dynamic modes

of vibration, static deformation modes are generally characterised by increasingly localisation of deformation and decreasing importance in the overall response.

4.1.2 Sensor placement

The POD analysis described in the previous subsection shows that to capture the overall displacement field, the sensors should be placed as to measure the Mode 1 elastic deformation field (longer base length), as well some localised displacement around the flat-jack. This can be obtained by a sensor setup as proposed in (Chisari, et al., 2018) and herein reported in Figure 13.

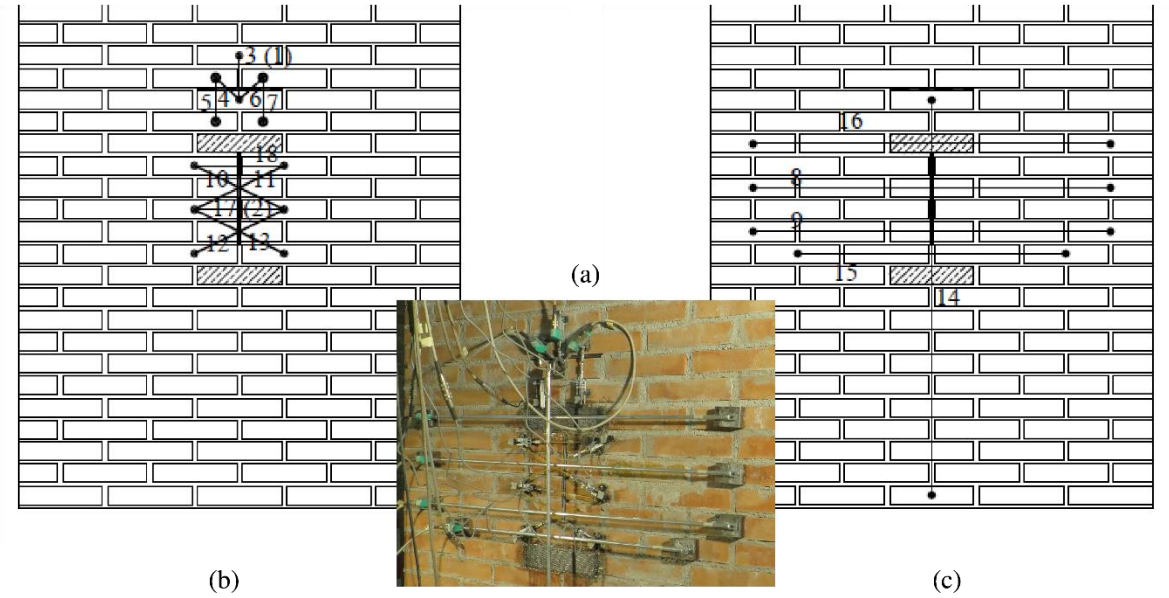


Figure 13. Instrumentation for displacement acquisition from the flat-jack test: (a) view of the setup around the vertical flat-jack; (b) LVDTs in proximity of the vertical slot; (c) LVDTs with longer base length (from (Chisari, et al., 2018)).

It is clear that, as theoretically shown in (Chisari, et al., 2015), a full-field acquisition methodology could greatly improve the representation of the deformation modes from the experimental data and decrease the error in the parameter estimation. However, such deformation field should capture both global and local displacement modes, and thus the application of novel multiscale DIC concepts (Bomarito, et al., 2018) could be exploited in this context.

5 Conclusions

In this paper, an in-depth analytical and numerical analysis on the stress and deformation states induced by a vertical flat-jack test is presented. This analysis complements the proposal of the test and appropriate data post-processing by means of inverse analysis in (Chisari, et al., 2018) as a means of calibrating an advanced mesoscale model for masonry structures. Two simplified elastic analytical models are described. In the first one, the masonry region influenced by the flat-jack is considered as a homogeneous material connected to the surrounding masonry by means of shear elastic springs. This allows the estimation of the shear stresses resulting from the test along the horizontal bed joint. An elastic numerical model validated the predictions given by the analytical model in two cases with different relative stiffness between brick and mortar. The analytical model developed predicts negligible stresses from a certain distance from flat-jack which depends on the relative deformability of masonry along the horizontal direction and bed joints in shear. This analysis clearly showed that the need for a complex restraint system as initially proposed in (Chisari, et al., 2015) can be relaxed provided that the flat-jack is sufficiently far from the free edge, leading to a remarkable simplification of the overall setup.

A second model, in which an infinite homogeneous elastic continuum is subjected to a uniform stress inside a vertical cut is subsequently described. It is derived exploiting the superposition of the effects for an infinite plate subjected to constant stress and the same with an elliptic hole. The case of vertical cut is treated as limit case of the elliptic hole. The model shows that the stress state originated from the vertical flat-jack is generally characterised by moderate stress values, with multi-axial compressive stresses in the proximity of the mid-point of the flat-jack. The exception to this is represented by the end points of the cut where a singularity in the horizontal tensile stress is predicted. This singularity clearly ceases if one considers finite thickness of the cut and material nonlinearity, but it still represents an indicator of possible crack onset in the wall. Similarly to the previous model, the perturbation induced by the test extinguishes at a distance equal to 1-1.5 times the flat-jack length. To reduce the

risk of vertical cracks propagation in the wall, which were experimentally observed in a preliminary test and would prevent the identification of nonlinear material properties of mortar, it is suggested to reinforce the bricks above and below the flat-jack by means of FRP strips.

Finally, the state of deformation is analysed by means of Proper Orthogonal Decomposition. The generation of a set of different numerical responses by varying the sought nonlinear material properties allows for an investigation on the different displacement fields and cracking patterns predicted by the model. It is shown that different deformation modes can occur in the test, characterised by either (i) an elastic deformation field, (ii) vertical cracks, (iii) diagonal cracks, (iv) local deformation in proximity of the flat-jack. The outcome of this analysis is the design of the most suitable sensor setup able to capture the main deformation modes of the test.

The theoretical analysis herein developed, and the experimental application described elsewhere show that vertical cracks along bricks and head joints can be partially avoided by the use of local FRP reinforcement, but even in such a case there is a deformation mode which could trigger a similar type of crack pattern. Special care and further study are thus recommended to ensure that the overall displacement field is characterised by diagonal cracks and can thus enable an effective estimation of mortar joint material parameters.

Acknowledgements

This research has been supported by the European Commission through the Marie Skłodowska-Curie Individual Fellowship "MultiCAMS – *Multi-level Model Calibration for the Assessment of Historical Masonry Structures*", Project no. 744400.

References

Andreotti, G., Graziotti, F. & Magenes, G., 2018. Detailed micro-modelling of the direct shear tests of brick masonry specimens: The role of dilatancy. *Engineering Structures,* Volume 168, pp. 929-949.

Anthoine, A., 1995. Derivation of the in-plane elastic characteristics of masonry through homogenization theory. *International Journal of Solids and Structures,* 32(2), pp. 137-163.

Atamturktur, S., Liu, Z., Cogan, S. & Juang, H., 2014. Calibration of imprecise and inaccurate numerical models considering fidelity and robustness: a multi-objective optimization-based approach. *Structural and Multidisciplinary Optimization,* 51(3), pp. 659-671.

Berto, L., Saetta, A., Scotta, R. & Vitaliani, R., 2002. An orthotropic damage model for masonry structures. *Int J Numer Methods Eng,* Volume 55, pp. 127-157.

Binda, L., Saisi, A. & Tiraboschi, C., 2000. Investigation procedures for the diagnosis of historic masonries. *Construction and Building Materials,* Volume 14, pp. 199-233.

Binda, L. & Tiraboschi, C., 1999. Flat-jack test as a slightly destructive technique for the diagnosis of brick and stone masonry structures. *International Journal for Restoration of Buildings and Monuments,* Volume 5, pp. 449-472.

Bomarito, G., Hochhalter, J. & Ruggles, T., 2018. Development of Optimal Multiscale Patterns for Digital Image Correlation via Local Grayscale Variation. *Experimental Mechanics,* 58(7), pp. 1169-1180.

Borri, A., Castori, G., Corradi, M. & Speranzini, E., 2011. Shear behavior of unreinforced and reinforced masonry panels subjected to in situ diagonal compression tests. *Construction and Building Materials,* 25(12), pp. 4403-4414.

Buljak, V., 2011. *Inverse Analyses with Model Reduction.* Berlin: Springer.

Calderini, C., Cattari, S. & Lagomarsino, S., 2010. The use of the diagonal compression test to identify the shear mechanical parameters of masonry. *Construction and Building Materials,* Volume 24, p. 677–685.

524 Caliò, I., 2011. *La prova di scorrimento con martinetto piatto (in Italian).* Bari (Italy), Proceedings of
525 the Fourteen Conference ANIDIS.
526 Cecchi, A., Milani, G. & Tralli, A., 2005. Validation of analytical multiparameter homogenization
527 models for out-of-plane loaded masonry walls by means of the finite element method. *Journal of*
528 *Engineering Mechanics,* 131(2), pp. 185-198.
529 Chisari, C., 2018. Tolerance-based Pareto optimality for structural identification accounting for
530 uncertainty. *Engineering with Computers (in press),* pp. 1-15.
531 Chisari, C., Macorini, L., Amadio, C. & Izzuddin, B., 2018. Identification of mesoscale model
532 parameters for brick-masonry. *International Journal of Solids and Structures,* Volume 146, pp. 224-
533 240.
534 Chisari, C., Macorini, L., Amadio, C. & Izzuddin, B. A., 2015. An Inverse Analysis Procedure for
535 Material Parameter Identification of Mortar Joints in Unreinforced Masonry. *Computers and*
536 *Structures,* Volume 155, pp. 97-105.
537 Chisari, C., Macorini, L., Amadio, C. & Izzuddin, B. A., 2016. Optimal sensor placement for structural
538 parameter identification. *Structural and Multidisciplinary Optimization,* 55(2), pp. 647-662.
539 Coker, E. G. & Filon, L. N. G., 1931. *A treatise on photo-elasticity.* s.l.:University Press.
540 Corradi, M., Borri, A. & Vignoli, A., 2003. Experimental study on the determination of strength of
541 masonry walls. *Construction and Building Materials,* Volume 17, pp. 325-337.
542 D'Ambrisi, A., Mariani, V. & Mezzi, M., 2012. Seismic assessment of a historical masonry tower with
543 nonlinear static and dynamic analyses tuned on ambient vibration tests. *Engineering Structures,*
544 Volume 36, pp. 210-219.
545 Fernández-Martínez, J., Fernández-Muñiz, Z., Pallero, J. & Pedruelo-González, L., 2013. From Bayes
546 to Tarantola: New insights to understand uncertainty in inverse problems. *Journal of Applied*
547 *Geophysics,* Volume 98, pp. 62-72.

548 Ferretti, F., Ferracuti, B., Mazzotti, C. & Savoia, M., 2019. Destructive and minor destructive tests on
549 masonry buildings: Experimental results and comparison between shear failure criteria. *Construction*
550 *and Building Materials,* Volume 199, pp. 12-29.
551 Gambarotta, L. & Lagomarsino, S., 1997. Damage models for the seismic response of brick masonry
552 shear walls. Part I: the mortar joint model and its applications. *Earthquake Engineering and Structural*
553 *Dynamics,* 26(4), pp. 423-439.
554 Garbowski, T., Maier, G. & Novati, G., 2011. Diagnosis of concrete dams by flat-jack tests and inverse
555 analyses based on proper orthogonal decomposition. *Journal of Mechanics of Materials and*
556 *Structures,* Volume 6, pp. 181-202.
557 Gentile, C. & Saisi, A., 2007. Ambient vibration testing of historic masonry towers for structural
558 identification and damage assessment. *Construction and Building Materials,* 21(6), pp. 1311-1321.
559 Gregorczyk, P. & Lourenço, P., 2000. A review on flat-jack testing. *Engenharia Civil,* Volume 9, p.
560 39–50.
561 Izzuddin, B. A., 1991. *Nonlinear dynamic analysis of framed structures.* Imperial College London:
562 PhD Thesis.
563 Kabanikhin, S., 2008. Definitions and examples of inverse and ill-posed problems. *Journal of Inverse*
564 *and Ill-Posed Problems,* 16(4), pp. 317-357.
565 Lotfi, H. R. & Shing, P., 1994. Interface model applied to fracture of masonry structures. *Journal of*
566 *structural engineering,* 120(1), pp. 63-80.
567 Lourenço, P. B., de Borst, R. & Rots, J. G., 1997. A plane stress softening plasticity model for
568 orthotropic materials. *International Journal for Numerical Methods in Engineering,* Volume 40, pp.
569 4033-4057.
570 Lourenço, P. B. & Rots, J. G., 1997. Multisurface Interface Model for Analysis of Masonry Structures.
571 *Journal of Engineering Mechanics,* 123(7), pp. 660-668.

572 Luciano, R. & Sacco, E., 1997. Homogenization technique and damage model for old masonry
573 material. *International Journal of Solids and Structures,* 34(24), pp. 3191-3208.
574 Macorini, L. & Izzuddin, B., 2011. A non-linear interface element for 3D mesoscale analysis of brick-
575 masonry structures. *International Journal of Numerical Methods in Engineering,* Volume 85, pp.
576 1584-1608.
577 Marastoni, D., Pelà, L., Benedetti, A. & Roca, P., 2016. Combining Brazilian tests on masonry cores
578 and double punch tests for the mechanical characterization of historical mortars. *Construction and*
579 *Building Materials,* Volume 112, pp. 112-127.
580 Mazzotti, C., Sassoni, E. & Pagliai, G., 2014. Determination of shear strength of historic masonries by
581 moderately destructive testing of masonry cores. *Construction and Building Materials,* Volume 54,
582 pp. 421-431.
583 Milani, G., Lourenço, P. & Tralli, A., 2006. Homogenised limit analysis of masonry walls, Part I:
584 Failure surfaces. *Copmuters and Structures,* 84(3-4), pp. 166-180.
585 Morbiducci, R., 2003. Non-linear parameter identification of models for masonry. *Int J Solids Struct,*
586 40(15), pp. 4071-4090.
587 Oberti, G., 1947. Ricerche sulle sollecitazioni preesistenti nelle strutture. *Giornale del Genio Civile,*
588 pp. 195-209.
589 Papa, E., 1996. Unilateral damage model for masonry based on a homogenization procedure. *Mech*
590 *Cohes-Frict Mater,* Volume 1, pp. 349-366.
591 Pelà, L., Cervera, M. & Roca, P., 2011. Continuum damage model for orthotropic materials:
592 Application to masonry. *Comput. Methods Appl. Mech. Engrg.,* Volume 200, pp. 917-930.
593 Sarhosis, V. & Sheng, Y., 2014. Identification of material parameters for low bond strength masonry.
594 *Engineering Structures,* Volume 60, pp. 100-110.

595 Sassoni, E., Mazzotti, C. & Pagliai, G., 2014. Comparison between experimental methods for
596 evaluating the compressive strength of existing masonry buildings. *Construction and Building*
597 *Materials,* Volume 68, pp. 206-219.
598 Sobol, I., 1967. Distribution of points in a cube and approximate evaluation of integrals. *U.S.S.R*
599 *Comput. Maths. Math. Phys,* Volume 7, pp. 86-112.
600 Tarantola, A., 2005. *Inverse Problem Theory and Methods for Model Parameter Estimation.*
601 Philadelphia: Society for Industrial and Applied Mathematics.
602 Tikhonov, A. & Arsenin, V., 1977. *Solution of Ill-posed Problems.* New York: Wiley.
603